








# The new missense G376V-TDP-43 variant induces late-onset distal myopathy but not amyotrophic lateral sclerosis

Julia Zibold,<sup>1,†</sup> Lola E. R. Lessard,<sup>2,3,†</sup> Flavien Picard,<sup>2,†</sup> Lara Gruijs da Silva,<sup>4,5,6,‡</sup> Yelyzaveta Zadorozhna,<sup>4,7,‡</sup> Nathalie Streichenberger,<sup>2,8</sup>  Edwige Belotti,<sup>2</sup> Alexis Osseni,<sup>2</sup> Andréa Emerit,<sup>2</sup> Elisabeth Errazuriz-Cerda,<sup>9</sup> Laurence Michel-Calemard,<sup>2,10</sup> Rita Menassa,<sup>2,10</sup> Laurent Coudert,<sup>2</sup> Manuela Wiessner,<sup>1</sup> Rolf Stucka,<sup>1</sup> Thomas Klopstock,<sup>1,11,12</sup> Francesca Simonetti,<sup>4,5,11</sup> Saskia Hutten,<sup>4</sup>  Takashi Nonaka,<sup>13</sup>  Masato Hasegawa,<sup>13</sup> Tim M. Strom,<sup>14</sup> Emilien Bernard,<sup>2,3</sup> Elisabeth Ollagnon,<sup>15</sup> Andoni Urtizberea,<sup>16</sup> Dorothee Dormann,<sup>4,12,17</sup> Philippe Petiot,<sup>18</sup>  Laurent Schaeffer,<sup>2</sup> Jan Senderek<sup>18</sup> and  Pascal Leblanc<sup>2§</sup>

†,‡,§These authors contributed equally to this work.

TAR DNA binding protein of 43 kDa (TDP-43)-positive inclusions in neurons are a hallmark of several neurodegenerative diseases including familial amyotrophic lateral sclerosis (fALS) caused by pathogenic TARDBP variants as well as more common non-Mendelian sporadic ALS (sALS). Here we report a G376V-TDP-43 missense variant in the C-terminal prion-like domain of the protein in two French families affected by an autosomal dominant myopathy but not fulfilling diagnostic criteria for ALS.

Patients from both families presented with progressive weakness and atrophy of distal muscles, starting in their fifth to seventh decade. Muscle biopsies revealed a degenerative myopathy characterized by accumulation of rimmed (autophagic) vacuoles, disruption of sarcomere integrity and severe myofibrillar disorganization. The G376V variant altered a highly conserved amino acid residue and was absent in databases on human genome variation. Variant pathogenicity was supported by *in silico* analyses and functional studies.

The G376V mutant increased the formation of cytoplasmic TDP-43 condensates in cell culture models, promoted assembly into high molecular weight oligomers and aggregates *in vitro*, and altered morphology of TDP-43 condensates arising from phase separation. Moreover, the variant led to the formation of cytoplasmic TDP-43 condensates in patient-derived myoblasts and induced abnormal mRNA splicing in patient muscle tissue.

The identification of individuals with TDP-43-related myopathy, but not ALS, implies that TARDBP missense variants may have more pleiotropic effects than previously anticipated and support a primary role for TDP-43 in skeletal muscle pathophysiology. We propose to include TARDBP screening in the genetic work-up of patients with late-onset distal myopathy. Further research is warranted to examine the precise pathogenic mechanisms of TARDBP variants causing either a neurodegenerative or myopathic phenotype.

1 Friedrich-Baur Institute at the Department of Neurology, University Hospital, LMU Munich, 80336 Munich, Germany

Received July 06, 2023. Revised November 20, 2023. Accepted November 26, 2023. Advance access publication December 11, 2023

© The Author(s) 2023. Published by Oxford University Press on behalf of the Guarantors of Brain.

This is an Open Access article distributed under the terms of the Creative Commons Attribution-NonCommercial License (<https://creativecommons.org/licenses/by-nc/4.0/>), which permits non-commercial re-use, distribution, and reproduction in any medium, provided the original work is properly cited. For commercial re-use, please contact [reprints@oup.com](mailto:reprints@oup.com) for reprints and translation rights for reprints. All other permissions can be obtained through our RightsLink service via the Permissions link on the article page on our site—for further information please contact [journals.permissions@oup.com](mailto:journals.permissions@oup.com).

- 2 Faculté de Médecine Rockefeller, Institut NeuroMyoGène-PGNM, Université Claude Bernard Lyon, 69008 Lyon, France
- 3 Service d'Electroneuromyographie et de pathologies neuromusculaires, Hôpital Neurologique Pierre Wertheimer, Hospices Civils de Lyon, 69677 Bron, France
- 4 Johannes Gutenberg University (JGU), Faculty of Biology, Institute of Molecular Physiology, 55128 Mainz, Germany
- 5 Graduate School of Systemic Neurosciences (GSN), LMU BioCenter, Department Biology II Neurobiology, 82152 Planegg-Martinsried, Germany
- 6 Center for Anatomy, Faculty of Medicine and University Hospital Cologne, University of Cologne, 50931 Cologne, Germany
- 7 International PhD Programme (IPP) of the Institute of Molecular Biology (IMB), 55128 Mainz, Germany
- 8 Département d'Anatomo-Pathologie, Groupement Hospitalier Est, Hospices Civils de Lyon, 69677 Bron, France
- 9 Plateforme d'imagerie CIQLE, 69008 Lyon, France
- 10 Service Biochimie et Biologie Moléculaire, Centre de biologie et pathologie Est, Hospices civils de Lyon, 69677 Bron, France
- 11 German Center for Neurodegenerative Diseases (DZNE), Munich Site, 81377 Munich, Germany
- 12 Munich Cluster for Systems Neurology (SyNergy), 81377 Munich, Germany
- 13 Dementia Research Project, Tokyo Metropolitan Institute of Medical Science, Tokyo 156-8506, Japan
- 14 Institute of Human Genetics, Klinikum rechts der Isar, Technical University Munich, 81675 Munich, Germany
- 15 Service de Génétique, Neurogénétique et Médecine Prédictive, Hôpital de la Croix-Rousse, Hospices Civils de Lyon, 69004 Lyon, France
- 16 Centre de Référence Neuromusculaire, Hôpital Marin—APHP, 64701 Hendaye, France
- 17 Institute of Molecular Biology (IMB), 55128 Mainz, Germany
- 18 Centre de santé Medicina Rockefeller, 69008 Lyon, France

Correspondence to: Pascal Leblanc  
Faculté de Médecine Rockefeller, Institut NeuroMyoGène-PGNM  
Université Claude Bernard 69008 Lyon, Lyon, France  
E-mail: pascal.leblanc@univ-lyon1.fr

Correspondence may also be addressed to: Jan Senderek  
Friedrich-Baur Institute at the Department of Neurology  
University Hospital, LMU Munich, 80336 Munich, Germany  
E-mail: jan.senderek@med.uni-muenchen.de

Laurent Schaeffer  
Institut NeuroMyoGène-PGNM, Faculté de Médecine Rockefeller  
Université Claude Bernard Lyon, 69008 Lyon, France  
E-mail: laurent.schaeffer@univ-lyon1.fr

**Keywords:** TDP-43; TARDBP; skeletal muscle; ALS; distal myopathy; protein aggregation; cryptic exons

## Introduction

TAR DNA binding protein of 43 kDa (TDP-43) encoded by the *TARDBP* gene is a ubiquitously expressed multifunctional DNA and RNA binding protein involved in key cellular processes such as transcription, RNA splicing and mRNA stability.<sup>1</sup> Under healthy conditions, TDP-43 is mainly a nuclear protein but it is known to shuttle between the nucleus and the cytoplasm where it is involved in the regulation of translational control, protein quality control, microRNA processing, mitochondrial autophagy, axonal and vesicle transport processes and stress response pathways (reviewed in Versluys *et al.*<sup>2</sup>). TDP-43 is a 414-amino acid protein that comprises a nuclear localization signal (NLS) and two RNA recognition motifs (RRMs). These motifs are flanked by a N-terminal region involved in oligomerization and a C-terminal low complexity domain (LCD), which shows homologies to prion-like domains (PrLD) of prion proteins.<sup>3–5</sup>

In pathological contexts, TDP-43 loses its nuclear localization and accumulates in cytoplasmic inclusions in brain and spinal

cord motor neurons and in glial cells of patients with sporadic or familial amyotrophic lateral sclerosis (s/fALS) or ALS with frontotemporal dementia (ALS-FTD).<sup>6</sup> In these inclusions, TDP-43 is hyperphosphorylated, poly-ubiquitinated and abnormally cleaved into aggregation-prone C-terminal fragments (CTFs) comprising the PrLD/LCD domain.<sup>7–10</sup> The LCD region has been demonstrated to play a crucial role in driving phase separation of TDP-43, which occurs through multivalent intermolecular interactions guiding the formation of high molecular weight oligomers or even (micrometre-sized) condensates.<sup>11,12</sup> These assemblies possibly represent intermediates in the transition from soluble protein species to mature aggregates.<sup>13</sup> Notably, almost all s/fALS-linked TDP-43 missense mutations reside in the LCD region, and many of them have been experimentally validated to alter phase separation and promote the formation of protein aggregates.<sup>11,13,14</sup> The identification of TARDBP variants in patients with s/fALS indicated that altered TDP-43 function can directly damage motor neurons and that

TDP-43 inclusions are not a mere secondary phenomenon related to neurodegeneration.<sup>6,15–17</sup>

TDP-43-positive inclusions are not restricted to neurons or glial cells but have also been discovered in the cytoplasm of immune cells,<sup>18–20</sup> fibroblasts<sup>21–23</sup> or skeletal muscle fibres<sup>24,25</sup> from ALS patients as well as in cells of subjects with limbic-predominant age-related TDP-43 encephalopathy (LATE)<sup>26</sup> or Alzheimer's and Parkinson's diseases.<sup>27,28</sup> TDP-43 inclusions were also identified in the skeletal muscles from patients with various skeletal muscle disorders including distal myopathies, myofibrillary myopathies with rimmed vacuoles, sporadic inclusion body myositis (sIBM) and IBM with Paget's disease and FTD.<sup>29–34</sup> TDP-43 was found to be a key regulator of myogenesis, and a recent study revealed that it is also involved in muscle regeneration through the formation of so-called myogranules.<sup>35</sup> Consequently, it is reasonable to speculate that TDP-43 loss- or gain-of-function due to misfolding/aggregation or up-regulation may be detrimental to normal muscle function.<sup>36</sup>

In the present study, we report the identification of two French families harbouring a G376V-TDP-43 missense variant, which segregated with autosomal dominant late-onset distal myopathy. Functional studies demonstrated that the G376V variant alters TDP-43 aggregation behaviour in transfected cells, patient-derived primary muscle cells and *in vitro* assays. Overall, these data strongly suggest that TARDBP missense variants can not only induce ALS and ALS/FTD pathologies but can also directly cause primary skeletal muscle disorders.

## Materials and methods

### Study participants and informed consent

The study population included nine affected and three unaffected individuals from two families referred to our institutions for assessment of an aetiologically unexplained distal myopathy. All participants gave informed consent for the extraction and use of primary care data, medical history-taking, clinical examinations, genetic studies and secondary use of biomaterials (blood/DNA samples, muscle biopsies and myoblast cultures) in the study. The study was conducted in accordance with national legislations and the ethical standards laid down in the 1964 Declaration of Helsinki and its later amendments. Research protocols were approved by Institutional Review Boards at the Faculté de Médecine Rockefeller Lyon and Ludwig-Maximilians-University Munich. Human biological samples and associated data and consents were obtained from Tissu-Tumorotheque Est Biobank (CRB) and the CBC Biotec (HCL Hospices Civils de Lyon) authorized by the French Ministry of Research (AC-2019-3465).

### Antibodies

The following primary antibodies were used: rabbit anti-TDP-43 antibodies [Cat. No. 12892-1-AP, western blotting (WB) 1:2000; Cat. No. 10782-2-AP WB 1:2000 and immunofluorescence (IF) 1:500] were from Proteintech. The rabbit anti-TDP-43 S409/S410-2 [Cat. No. TIP-PTD-P02; immunohistochemistry (IHC) 1:1000] was from Cosmo Bio. The mouse anti-SQSTM1/p62 (Cat. No. 610833 3P62, IHC 1:500) was from BD Biosciences. The rabbit anti-GAPDH (mAb#2118, WB 1:10 000) was from Cell Signaling Technology. The rat anti-HA (3F10, Cat. No. 11867423001; WB 1:2000) was from Merck.

The following secondary antibodies were used for WB: anti-Rabbit (NA934; GE Healthcare UK) and the anti-Rat (sc-2956; Santa Cruz) labelled with peroxidase were used at 1:10 000.

For IF experiments, the donkey anti-Rabbit Alexa-Fluor 488 (A21206) was purchased from Molecular Probe and was used at 1:1000.

### Histopathological analysis

Muscle biopsy specimens were taken at sites distant from position of placement of EMG needles. A portion of the tissue sample was immediately frozen in cooled isopentane and 7 µm cryosections were processed for histology: haematoxylin phloxin saffron (HPS) and Gomori trichrome stainings as well as nicotinamide adenosine dinucleotide tetrazolium reductase (NADH-TR) and cytochrome c oxidase (COX) reactions. A second portion of the tissue sample was formalin-fixed, embedded in paraffin and sectioned for an automated IHC analysis on a BenchMark XT (Ventana Medical Systems). Anti-SQSTM1/p62 and anti-phospho-TDP-43 (pS409/410) were used as primary antibodies and antigen-antibody complexes were detected with the help of biotinylated secondary antibodies, avidin-biotin-peroxidase complexes and Ventana DAB detection and amplification kits. Digital image capture was performed using an Axio Scan.Z1 microscope (Zeiss) at the CIQLE platform of the Faculty of Medicine of Lyon, France.

### Transmission electron microscopy analysis

Transmission electron microscopy analyses were performed as previously described.<sup>37</sup> Biopsy samples were fixed with 2% glutaraldehyde [Electron Microscopy Sciences (EMS)] in 0.1 M sodium cacodylate buffer (pH 7.4). After washing three times in 0.2 M sodium cacodylate buffer, tissues were post-fixed with 2% osmium tetroxide (EMS) at room temperature for 1 h. Samples were then dehydrated in a graded series of ethanol at room temperature, transferred to propylene oxide (EMS) and embedded in Epon epoxy resin (EMS). After polymerization, ultrathin sections (100 nm) were cut on a UC7 ultramicrotome (Leica) and collected on 200 mesh grids. Sections were stained with uranyl acetate and lead citrate prior to analysis on a JEM-1400 (Jeol) transmission electron microscope equipped with an Orius 600 camera and digital micrograph.

### Genome-wide linkage analysis

DNA samples from Family A were hybridized to Affymetrix GeneChip Human Mapping NspI 250 K arrays. Genotypes were called with GeneChip Genotyping Analysis Software and default thresholds. Parametric multipoint logarithm of the odds (LOD) scores were calculated with MERLIN assuming a dominant mode of inheritance and a frequency of the disease allele of 0.0001.

### Exome sequencing

Whole-exome sequencing of Individual A-III:7 was performed on a Genome Analyzer HiSeq 2000 system (Illumina) after using the SureSelect Human all Exon 50 Mb kit v4 (Agilent) for in-solution enrichment of exon and adjacent intron sequences. Read alignment was performed with BWA v.0.5.8 to the human genome assembly hg19 and single-nucleotide variants and small indels were called with SAMtools v.0.1.7. Variant annotation was performed with custom Perl scripts, integrating data from dbSNP135 and the UCSC Genome Browser Known Genes track. Further analysis was restricted to heterozygous non-synonymous variants excluding HapMap single-nucleotide polymorphisms present in dbSNP135 with an average heterozygosity >0.02 and variants present in >4 of >12 000 in-house exomes from individuals with unrelated diseases.

## Sanger sequencing

Segregation studies were performed by Sanger sequencing. Oligonucleotide primer sequences for PCR amplification are available upon request. Sequences of PCR-amplified DNA fragments were identified by BigDye Terminator Ready Reaction Cycle Sequence Kit and capillary electrophoresis (Applied Biosystems).

## Cell culture

The human embryonic kidney cell line HEK293T was obtained from the American Type Culture Collection (ATCC). The U2OS cell line was kindly provided by Dr Delphine Poncet (INMG-PGNM Lyon). Cells were cultured in Dulbecco's modified Eagle medium (DMEM)-GlutaMAX high glucose + pyruvate supplemented with 10% of fetal bovine serum (FBS) and penicillin/streptomycin (P/S). The human SH-SY5Y neuroblastoma cell line was obtained from Sigma-Aldrich. Cells were cultured in DMEM/F12 GlutaMAX supplemented with 10% of FBS, P/S and non-essential amino acid medium (NEAA). Human primary myoblasts from non-disease control individuals (Individuals Y691/CT1 and Y711/CT2; both males, aged 68 and 71 years, respectively) and patients with the G376V distal myopathy (Patients Y723/FA-IV:6 and V690/FB-IV:4; both males with an age of 71 and 82 years, respectively) were obtained from the Tissu-Tumorothèque Est Biobank (CRB-HCL) and the CBC Biotech-HCL authorized by the French Ministry of Research (AC-2019-3465). Myoblasts were cultured in proliferating culture medium as previously described<sup>38</sup> (KMEM: one volume of M199, four volumes of DMEM-GlutaMAX high glucose + pyruvate, 20% FBS, 25 µg/ml fetuin, 0.5 ng/ml β-FGF, 5 ng/ml EGF, 5 µg/ml insulin, P/S). Differentiation of myoblasts into myotubes was induced by switching to DIFF-medium (one volume of M199, four volumes of DMEM, 2% horse serum and 10 µg/ml insulin). All cell culture media and reagents were purchased from Gibco-Thermo Fisher Scientific.

## Expression constructs

Mammalian expression constructs for HA-tagged wild-type, G298S, M337V and Q343R TDP-43 (in pcDNA3) and for GFP-tagged wild-type, G294A, G298S and Q331K TDP-43 (in pEGFPC1) were provided by Takashi Nonaka.<sup>39,40</sup> The QM516B2-GFP-TDP-43-WT, -G294A, -G298S and -Q331K lentiviral constructs were created by subcloning the GFP-TDP-43 from pEGFPC1 into the QM516B2 lentivector (System Biosciences). The pcDNA3-HA-TDP-43-G376V construct was created by PCR mutagenesis. The QM512B2-GFP-TDP-43-G376V construct, the pLVX-tetOne-Puro-HA-TDP-43-WT, -G376V and -G376D constructs, and the pcDNA3-HA-TDP-43-G376D construct were created by gene synthesis and mutagenesis (Genscript).

The psPAX2 plasmid, which is a second generation lentiviral packaging construct encoding HIV-1 Gag and GagPol, and the pMDG2 plasmid encoding the vesicular stomatitis envelope glycoprotein (VSVg) were kindly provided by Didier Trono (EPFL). The pLKO1 constructs encoding small hairpin RNAs (shRNA) directed against human TARDBP (TDP-43#38 TRCN0000016038; TDP-43#40 TRCN0000016040) were purchased from Sigma-Aldrich (Mission shRNA plasmid DNA).

The negative shRNA control pLKO1 (shCT) was kindly provided by Clotilde They and previously described.<sup>38,41</sup>

The bacterial expression constructs pJ4M-wild-type TDP-43-TEV-MBP-His<sub>6</sub> was obtained from Addgene (Plasmid#104480) and was first described in Wang et al.<sup>42</sup> The G376V and G376D variants were created by site-directed mutagenesis.

Sequence integrity of all constructs was verified by Sanger sequencing.

## Transient and stable transfections

One day prior to transfection, HEK293T cells were plated at a density of 400 000 cells per well in six-well plates in presence or absence of coverslips. Cells were transfected with 1–2 µg of constructs encoding HA- or GFP- fused wild-type or G376V TDP-43 using Fugene HD reagent (Promega), according to the manufacturer's protocol. Transfected cells were analysed 48–72 h after transfection.

U2OS cell lines stably expressing HA-TDP-43-WT, -G376V and -G376D were obtained by transfection of 2 µg of pLVX-tetOne-Puro-HA-TDP-43-WT, -G376V or -G376D using Fugene HD and subsequent selection of cells with 1 µg/ml of puromycin.

## RNA interference and lentivector vector production

This methodology, which has been previously described,<sup>43</sup> is depicted in the [Supplementary material](#).

## RNA extraction and RT-PCR experiments

This methodology is depicted in the [Supplementary material](#).

## Induction of osmotic stress

Transfected HEK293T cells, primary myoblasts or differentiated myotubes were cultured in the appropriate culture medium containing 400 mM D-sorbitol (Euromedex) for 1–3 h at 37°C. Cells were washed in PBS and then fixed for direct green fluorescent protein (GFP)-fluorescence or IF confocal microscopy.

## Direct fluorescence and immunofluorescence confocal microscopy imaging

Primary myoblasts and myotubes were grown on poly-lysine or Matrigel™-coated glass coverslips or alternatively in four-wells-Labtek systems (Thermo Fischer Scientific). Cells were washed with 1× PBS and fixed with 2% paraformaldehyde (PFA) in 1× PBS at room temperature for 15 min. Cells were then permeabilized with 0.2% Triton X-100 (Sigma-Aldrich) for 5 min at room temperature and blocked with 1× PBS containing 2% bovine serum albumin (BSA) for 1 h. Primary myoblasts and myotubes were labelled with the an anti-TDP-43 primary antibody (Cat. No. 10782-2-AP; 1:500) in 1× PBS containing 2% of BSA overnight at 4°C. After extensive washing steps in 1× PBS, cells were stained for 1 h at room temperature with a secondary antibody coupled to Alexa Fluor 488. After washing with 1× PBS, Labteks were mounted with Immu-Mount™ medium (Thermo Scientific) or, in FluorSave™ reagent (Millipore). HEK293T cells transfected with constructs encoding EGFP-TDP-43 were fixed in 4% PFA for 10 min, washed in 1× PBS, and stained with DAPI. After additional washings, coverslips were mounted with Immu-Mount™ medium for direct fluorescence microscopy. Digital image capture was performed using a confocal LSM-880 microscope (Zeiss) at the CIQLE platform from the Faculty of Medicine of Lyon, France. Images were analysed using the ImageJ software (version 1.8).

## Sarkosyl fractionation and immunoblotting

Two to three days after transfection, cells were harvested and lysed in 350 µl of homogenization buffer [HB; 10 mM Tris-HCl, (pH 7.5),

0.8 M NaCl, 1 mM EGTA, 1 mM DTT] supplemented with 1% *N*-laurylsarcosine sodium salt (sarkosyl), protease inhibitors (Complete, EDTA-free; Roche) and phosphatase inhibitors (PhosphoStop, Roche). Cell lysates were briefly sonicated and then ultracentrifuged at 100 000g for 30 min at room temperature in a TLA-100.3 rotor (optima max ultracentrifuge, Beckman). The supernatant was recovered as the sarkosyl-soluble fraction and mixed with 5× concentrated sample buffer [312.5 mM Tris-HCl (pH 6.8), 25% 2-mercaptoethanol, 50% glycerol, 10% sodium dodecylsulphate (SDS), bromophenol blue]. The pellet was washed in homogenization buffer, resuspended in 1× sample buffer, sonicated for solubilization and then used as the sarkosyl-insoluble fraction. Samples were separated by 12% SDS-PAGE gels, transferred on 0.45 µm polyvinylidene difluoride membrane (PVDF; Millipore), and probed with anti-HA and anti-GAPDH primary antibodies overnight at 4°C. After three washes with TBS-Tween buffer (Interchim), membranes were probed with HRP-conjugated secondary antibodies for 1 h at room temperature. Membranes were then washed as previously described, and signals were detected using the ECL-prime (GE Healthcare) detection kit and a ChemiDoc™ Touch imaging system. Quantification of immunoblots was done using the Image Lab software (Bio-Rad).

### TDP-43-MBP-His<sub>6</sub> protein expression and purification

TDP-43-MBP-His<sub>6</sub> wild-type, G376V or G376D variants, and His<sub>6</sub>-TEV protease were expressed and purified as previously described<sup>44,45</sup> or with modifications in the composition of the lysis buffer [50 mM Tris pH 8, 1 M NaCl, 10 mM imidazole, 10% (v/v) glycerol, 4 mM β-mercaptoethanol and 1 µg/ml each of aprotinin, leupeptin hemisulphate and pepstatin A] and the size exclusion chromatography purification buffer [50 mM Tris pH 8, 300 mM NaCl, 5% (v/v) glycerol supplemented with 2 mM TCEP].

### In vitro phase separation and aggregation assays

Experimental procedures were previously described<sup>44</sup> and are depicted in the [Supplementary material](#).

### Statistical analysis

Data are shown as mean ± standard error of the mean (SEM). Data were analysed in GraphPad Prism (version 9.0.0 for MacOS, GraphPad Software, San Diego, www.graphpad.com). A *P*-value <0.05 was considered statistically significant.

## Results

### Characterization of two French families with hereditary distal myopathy

Here we describe two families (Families A and B) presenting with late-onset autosomal dominantly inherited distal myopathy (Fig. 1A). Both families originated from the same region in France; however, there was no known ancestral connection. Seven affected subjects from Family A (Patients FA-III:5, FA-III:7, FA-III:9, FA-III:11, FA-III:16, FA-IV:3 and FA-IV:6; Table 1), three unaffected individuals (Individuals FA-III:14, FA-IV:2 and FA-IV:5) and two affected patients from Family B (Patients FB-IV:4 and FB-V:1; Table 1) underwent a physical examination in our centre (HCL, Hôpital Neurologique P. Wertheimer). The health status of additional

relatives was reported by the probands and extracted from available medical records. None of the families had a history of ALS or FTD.

All nine examined affected individuals had normal motor development and their motor capacities remained unremarkable until clinical symptoms started at a median [interquartile range (IQR)] age of 50 (45–50) years. The median (IQR) disease duration was 20 (13–34) years; five patients died after a median (IQR) disease duration of 28 (15–35) years. Initial symptoms were distal muscle weakness and atrophy that started in the upper extremities in four (44%) patients, in the lower limbs in two (22%) patients and simultaneously in the upper and lower extremities in three (33%) patients. Weakness in the upper extremities predominantly affected hand and finger extensors, while the anterior and lateral muscles of the leg were the most severely affected muscles of the lower extremities (Fig. 1B–F). Asymmetric muscle involvement occurred in six (67%) patients. Symptoms progressively worsened over time and three (33%) patients required ambulatory support at their last visit. One of the nine affected individuals became wheelchair-bound after the age of 80 years. Additional features were dysphagia (89%) manifesting at a mean (IQR) age of 62 (61–65) years, dyspnoea (89%) first noted at a mean (IQR) age of 59 (55–66) years, and diaphragmatic palsy (67%) with onset at a mean (IQR) age of 70 (64–70) years. There were no signs of pyramidal tract dysfunction such as spasticity, hyperreflexia or plantar responses. Sensory exam was unremarkable except for malleolar hypoesthesia in aged patients. Even at advanced age (mean age at the end of follow-up 70 years), none of the patients showed symptoms or signs of executive dysfunction, language impairments or behavioural changes evocative of cognitive deficits or dementia.

In all nine patients tested, needle EMG showed myopathic patterns in affected muscles, including fibrillations, positive sharp waves at rest, and polyphasic motor unit potentials of short duration and low amplitude during voluntary contraction. No myotonic discharge, no fasciculation or neuropathic changes were found. Nerve conduction studies were unremarkable as well. MRI (four patients) and CT (three patients) showed marked distal muscle atrophy with relative sparing of the thigh muscles; in the upper limbs, muscle atrophy was predominant in the posterior forearm muscles; in the lower limbs, muscle atrophy was most prominent in the anterior leg muscles (Fig. 1G–O). Seven of eight tested patients had restrictive lung function with forced vital capacity (FVC) decreased by a median (IQR) percentage of 44% (33–55) of reference values. Cardiac disease occurred in three patients: one patient had hypertrophic cardiomyopathy, a second patient presented with atrial fibrillation with unremarkable cardiac ultrasound, and the third one had asymptomatic left bundle branch block with normal cardiac ultrasound and ECG Holter (Table 1). Serum creatine kinase (CK) levels were within normal ranges in five patients (62.5%) or moderately elevated to a maximum of 500 IU/l in three patients (37.5%).

Patients FA-II:2, FA-II:5, FA-II:8, FA-III:2 and FA-IV:1 from Family A were not examined in our reference centre (Hospices Civils de Lyon, Hôpital Neurologique P. Wertheimer). However, according to their relatives, these individuals were affected by progressive distal muscle weakness starting in adulthood. Patients FA-II:2, FA-II:5 and FA-II:8 had died at the age of 75, 65 and 68 years, respectively. Patient FA-III:2, currently 84 years old, was reported to present with distal muscle involvement occurring after the age of 60 years. Patient FA-IV:4 was reported to have no overt muscle weakness or atrophy at the age of 57 years; however, she had restrictive lung disease (FVC decreased by 30%).

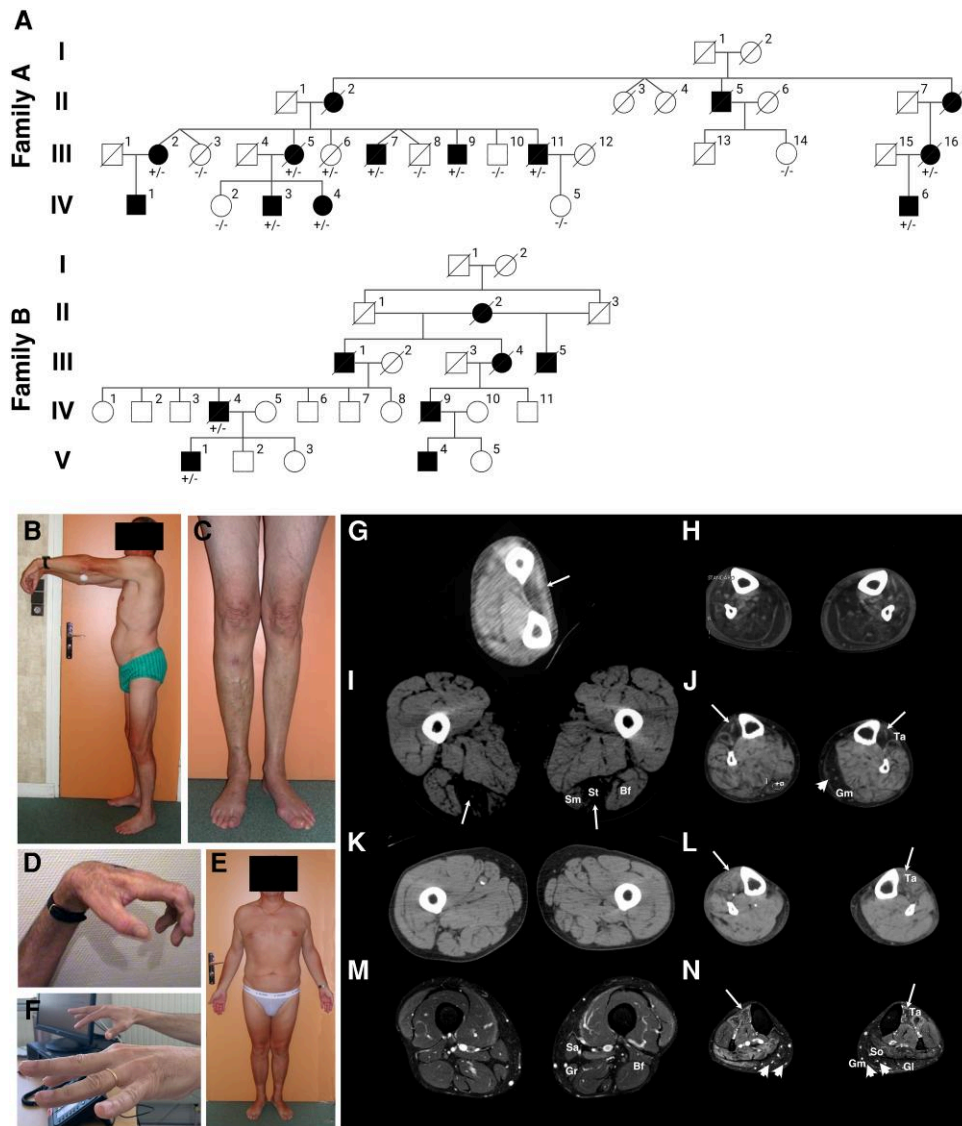


**Figure 1** Two families presenting with late-onset distal myopathy with autosomal dominant inheritance. (A) Family trees. Pedigrees of Family A (top) and Family B (bottom). Squares represent males and circles represent females. Black filled symbols correspond to patients suffering from distal myopathy. *TARDBP* genotypes of individuals from whom a DNA sample was available are given below the pedigree symbols. +/- indicates heterozygous for the *TARDBP* variant; -/- indicates homozygous for wild-type. (B-F) Clinical findings. (B) Individual FA-III:11, age 67 years, presented with bilateral upper limb extensor muscle deficit resulting in wrist drop. (C) Individual FA-III:5, age 70 years, presented with asymmetric atrophy of the anterior compartment of the lower leg muscles. (D) Individual FA-III:9, age 72 years, presented with marked bilateral weakness of hand and finger extensors. (E) Individual FA-IV:6, age 49 years, presented with bilateral atrophy of the tibialis anterior muscles. (F) Individual FB-V:1, age 53 years, presented with bilateral weakness of hand and finger extensors, most prominent on the index extensors. (G-N) Skeletal muscle imaging findings. (G and H) Skeletal muscle CT scans of Individual FA-III:9, age 72 years, showed atrophy of posterior forearm muscles (arrow in G) and diffuse atrophy of anterior and posterior lower leg muscles (H). (I and J) Skeletal muscle CT scans of Individual FA-IV:6, age 51 years, showed discrete atrophy of posterior thigh muscles (arrows in I) and severe atrophy of the tibialis anterior muscles (arrows in J) and the left gastrocnemius medialis muscle (arrowhead in J). (K and L) Skeletal muscle CT scans of Individual FB-IV:4, age 73 years, showed relative sparing of the thigh muscles (K) and symmetric involvement of tibialis anterior (arrows in L). (M and N) Skeletal muscle T<sub>2</sub>-weighted Dixon MRI scans of Individual FB-V:1, age 53 years, showed bilateral fatty infiltration and atrophy of thigh muscles, especially in the posterior group (M), and of lower leg muscles, predominantly affecting the gastrocnemius medialis and soleus (arrowheads in N) as well as the tibialis anterior muscles (arrows in N). Bf = biceps femoris; Gl = gastrocnemius lateralis; Gm = gastrocnemius medialis; Gr = gracilis; Sa = sartorius; Sm = semi-membranosus; So = soleus; St = semi-tendinosus; Ta = tibialis anterior.

According to their relatives, Individuals FB-II:2, FB-III:1, FB-III:4 and FB-III:5 from Family B, who were already deceased at the time of this study, had also been affected by a distal myopathy. Their age of death was unknown. Patient FB-IV:9 had been examined in another hospital, and his medical records indicated that he had experienced asymmetric distal muscle weakness occurring

before the age of 65 years, had been able to walk without limitations at the age of 75 years, and had shown a myopathic EMG pattern.

None of the additional affected individuals, whose medical data were provided by their family members, had a reported history of cognitive deficits or dementia.

Table 1 Clinical characteristics of affected individuals carrying the TDP-43 G376V variant

Family	Family A						Family B		
	Individual	FA-III:5	FA-III:7	FA-III:9	FA-III:11	FA-III:16	FA-IV:3	FA-IV:6	FB-IV:4
Sex/current age <sup>a</sup> , years	F/ <sup>†</sup> > 80	M/ <sup>†</sup> > 66	M/ <sup>†</sup> 78	M/ <sup>†</sup> 84	F/ <sup>†</sup> 85	M/63	M/72	M/ <sup>†</sup> 80	M/58
Age at symptoms onset, years	45	54	50	50	69	50	49	40	40
First symptoms	Distal UL	Distal UL + LL	Distal UL	Distal UL + LL	Distal UL + LL	Distal UL	Distal LL	UL	Distal LL
Disease duration, years	>35	>12	28	34	16	13	>23	40	>18
Time to all four extremities, years	10	0	5–10	0	0	5	5	10	10
Asymmetric involvement	Yes	No	Yes	Yes	No	Yes	Yes	No	Yes
Impairment of ambulation <sup>b</sup>	+	+	++	+++	+	+	+	++	++
Dysphagia (age, years)	Yes (66)	Yes (62)	Yes (60)	Yes (63)	Yes (73)	Yes (61)	No	Yes	No
Exertional dyspnoea (age, years)	Yes (65)	Yes (62)	Yes (55)	Yes (56)	Yes (73)	Yes (55)	Yes (55)	Yes (70)	No
Diaphragmatic palsy (age, years)	Yes (70)	Yes (62)	Yes (72)	Yes (70)	No	Yes (55)	No	Yes (70)	No
Cardiac involvement (age, years)	No	No	No	HCM	AF	No	LBBB	No	No <sup>c</sup>
CK level (IU/l)	157	N	N	500	173	NP	500	N	430
Electromyography	Myopathic	NP	Myopathic	Myopathic	Myopathic	NP	Myopathic	Myopathic	Myopathic
Reduction of FVC (%)	–20	–28	–70	–50	NP	–37	–60	–44	No
Cognitive deficit	No	No	No	No	No	No	No	No	No

AF = atrial fibrillation; CK = creatine kinase; F = female; FVC = forced vital capacity; HCM = hypertrophic cardiomyopathy; LBBB = left bundle branch block; LL = lower limbs; M = male; N = within normal range; NA = not applicable; NP = not performed; UL = upper limbs; UK = unknown.

<sup>†</sup>Deceased.

<sup>a</sup>Current age for living individuals or age of death.

<sup>b</sup>Impaired ambulation at last visit: – = normal gait; + = walks with difficulties; ++ = ambulation with support; +++ = wheelchair-bound.

<sup>c</sup>One episode of ventral tachycardia.

## Patients display vacuolar myopathy associated with SQSTM1/p62- and TDP-43-positive inclusions

Analysis of muscle biopsies of three patients (Patients FA-IV:6; FB-IV:4 and FB-V:1) revealed chronic myopathic changes, including myofibre atrophy, few necrotic myofibres, fibrosis and centralized nuclei (Supplementary Table 1 and Fig. 2A). Sarcoplasmic rimmed vacuoles were observed on HPS and Gomori trichrome staining [Fig. 2A(i–iii) and Supplementary Fig. 1A]. Acid phosphatase activity was increased (Supplementary Fig. 1B and C), indicating abnormal lysosomal activity. COX and NADH staining identified well demarcated central sarcoplasmic areas of reduced or absent mitochondrial enzyme activity (Supplementary Fig. 2A–F) as well as local accumulations of mitochondria were also observed (Supplementary Fig. 2B and E). There were no signs of neurogenic atrophy, such as fibre type grouping or target fibres. Additional immunohistochemical examination of muscle biopsies obtained from Patients FA-IV:6, FB-IV:4 and FB-V:1 demonstrated sarcoplasmic inclusions that stained positive for SQSTM1/p62 and phosphorylated TDP-43. These inclusions were associated with rimmed vacuole-like structures, providing additional evidence to support the diagnosis of a degenerative vacuolar myopathy [Fig. 2A(iv–ix)]. Transmission electron microscopy (TEM) confirmed the presence of intracellular vacuoles with ultrastructural characteristics of autophagic compartments [Fig. 2B(i, ii and iv)]. Concomitantly, distorted and dissociated Z-disc structures indicated disruption of sarcomere integrity with severe myofibrillar disorganization [Fig. 2B(i, iii and iv)].

## Exome sequencing identified a G376V-TDP-43 variant in patients with hereditary distal myopathy

Transmission of the disease in both families was consistent with autosomal dominant inheritance (Fig. 1A). Genome-wide linkage analyses using DNA from five affected members of Family A identified genomic interval on six chromosomes for which the maximum LOD of 1.49 was obtained. Subsequently, exome

sequencing of Patient FA-III:11 yielded 188 rare non-synonymous variants in genes not previously related to hereditary myopathy. Five of these variants fell into regions highlighted by linkage analysis. Segregation studies using DNA from further affected family members excluded all variants except for a previously unreported c.1127G>T substitution in the TARDBP gene, encoding a mutant TDP-43 protein harbouring a G376V variant protein (Fig. 3A). Duo exome sequencing in Patients FB-IV:4 and FB-V:1 from Family B identified the same heterozygous c.1127G>T TARDBP substitution, which was subsequently confirmed by Sanger sequencing (Fig. 3A and B). This variant was not present in databases covering human genome variation such as gnomAD,<sup>46</sup> ESP6500<sup>47</sup> and 1000G<sup>48</sup> (Supplementary Table 2) and affected an evolutionary conserved amino acid residue (Fig. 3C and Supplementary Table 3) inside the C-terminal LCD domain. G376 is part of a conserved sequence flanked by two steric zipper motifs (370-GNNSYS-375 and 396-GFNGGFG-402; Fig. 3D), both having a pivotal role on the pathogenic aggregation process of TDP-43.<sup>49</sup> Ten of 12 pathogenicity prediction algorithms classified the G376V amino acid substitution as a potentially damaging variant (Supplementary Table 4).

## The G376V variant reduces TDP-43 solubility in cells

Most reported TDP-43 variants associated with ALS and ALS/FTD target the LCD domain and some of them were reported to promote cytoplasmic TDP-43 aggregation.<sup>6</sup> Therefore, we first determined the impact of the G376V amino acid substitution on TDP-43 propensity to aggregate formation. We transfected HEK293T cells with constructs encoding HA-tagged wild-type or G376V-mutant TDP-43 and then examined the solubility of TDP-43 species by harvesting and lysing the cells in the presence of 1% sarkosyl, a detergent known to enhance the detection of alterations in TDP-43 solubility.<sup>43</sup> Sarkosyl-soluble and sarkosyl-insoluble pellet fractions were recovered by ultracentrifugation and analysed by immunoblotting using antibodies directed against the HA tag (for detection of tagged

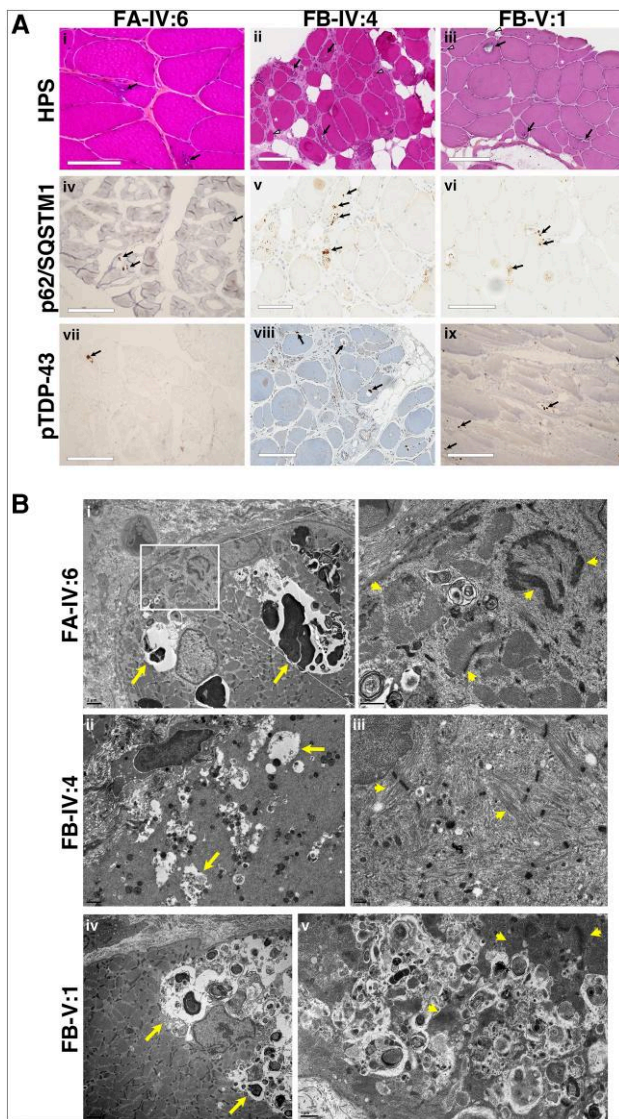


**Figure 2** Histopathological, immunohistochemical and ultrastructural analyses of muscle biopsies. [A(i–iii)] Light microscopic analysis. Haematoxylin-phloxine-saffron (HPS) staining of muscle biopsies from Individuals FA-IV:6, FB-IV:4 and FB-V:1 showed chronic degenerative changes, including atrophic myofibres (empty arrowheads), myofibre necrosis (number signs), centralized nuclei (asterisks), fibrosis and sarcoplasmic rimmed vacuoles (arrows). Scale bars = 100  $\mu$ m (i) or 200  $\mu$ m (ii and iii). [A(iv–ix)] Immunohistochemical analysis. Immunostaining for SQSTM1/p62 [A(iv–vi)] and phosphorylated TDP-43 [pTDP-43; A(vii–ix)] of muscle biopsies from Individuals FA-IV:6, FB-IV:4 and FB-V:1 revealed sarcoplasmic inclusions associated with vacuoles (arrows). Note that samples from Individuals FA-IV:6 and FB-V:1 showed massive structural alterations due to freeze-thaw damage. Scale bars = 100  $\mu$ m (v) or 200  $\mu$ m (iv and vi–ix). [B(i–v)] Ultrastructural analysis. Transmission electron microscopy of muscle biopsy samples from Patients FA-IV:6, FB-IV:4 and FB-V:1 revealed an accumulation of autophagic vacuoles in the sarcoplasm (arrows) and disruption of sarcomeric integrity associated with distortion of Z-disc structures (arrowheads). Scale bars = 0.5  $\mu$ m (iii), 1  $\mu$ m (i, right, ii and v), or 2  $\mu$ m (i left and iv). B(ii) Right: The boxed region from B(ii), left at higher magnification.

TDP-43) and GAPDH (as a loading control). HA-tagged G376V-TDP-43 was substantially enriched in the sarkosyl-insoluble fraction compared to the wild-type protein (Fig. 4A and B).

### G376V-TDP-43 assembles into morphologically distinct condensates and enhances TDP-43 aggregation *in vitro*

To examine whether the G376V variant alters the ability of TDP-43 to undergo phase separation or liquid-to-solid phase transitions, we expressed full-length wild-type and G376V-mutant TDP-43 fused to a solubilizing maltose binding protein (MBP)-tag and a His<sub>6</sub>-tag in *Escherichia coli*.<sup>42,44</sup> Already during protein purification by size exclusion chromatography, we noted that the G376V variant showed more abundant TDP-43 oligomers compared to the wild-type protein (Supplementary Fig. 3A and B). Phase separation of TDP-43 was initiated by treatment with Tobacco Etch Virus (TEV) protease, which cleaves off the solubilizing MBP-tag, thereby allowing TDP-43 condensation. Turbidity measurements of wild-type and G376V-TDP-43 demonstrated a similar concentration-dependent increase in phase separation, though values at low protein concentrations tended to be higher for the G376V variant (Fig. 4C). Bright-field microscopy revealed that wild-type TDP-43 formed large, rounded condensates, similar to what has been previously reported,<sup>50</sup> which could indicate that the condensates have a droplet-like nature and grow by fusion. In contrast, G376V-TDP-43 condensates were much smaller and had an irregular, amorphous shape and were often found in chain-like arrangements (Fig. 4D) suggesting that they tend to stick to each other. Next, we conducted semi-denaturing detergent agarose gel electrophoresis (SDD-AGE) experiments to monitor TDP-43 aggregation kinetics.<sup>44</sup> Over a 5-day period, we found that the G376V variant displayed more rapid oligomerization and formation of SDS-resistant higher molecular weight TDP-43 species compared to the wild-type protein (Fig. 4E).

### The G376V-TDP-43 variant is more aggregation-prone compared to ALS-associated variants

Another missense variant affecting TDP-43 codon G376, a glycine to aspartic acid substitution (G376D), has been previously reported to cause rapidly progressive ALS.<sup>51–59</sup> Consequently, we sought to compare predicted aggregation propensities of wild-type TDP-43, G376V-TDP-43 and G376D-TDP-43. The *in silico* prediction tool PLAAC (prion-like amino acid composition)<sup>60</sup> yielded a higher aggregation propensity score for myopathy-associated G376V-TDP-43 (PAPA score: 0.060) than for wild-type TDP-43 (PAPA score: 0.043) and ALS-associated G376D-TDP-43, which even scored lower than the wild-type (PAPA score: 0.029) (Supplementary Fig. 4A and B). Similarly, the ZipperDB algorithm,<sup>61</sup> which evaluates peptide sequences for their likelihood to form self-complementary  $\beta$ -strands termed ‘steric zippers’ that drive self-assembly, predicted that the G376V mutation but not the G376D variant introduces steric zipper motifs that could increase TDP-43 aggregation (Supplementary Fig. 4C).

To validate these findings experimentally, HEK293T cells were transfected with constructs encoding HA-tagged wild-type, G376V-mutant or the G376D-mutant TDP-43. Sarkosyl-soluble and sarkosyl-insoluble fractions were isolated and analysed by immunoblotting, as described above. Again, the G376V variant was more prone to form insoluble TDP-43 aggregates compared to both the G376D variant and the wild-type TDP-43, while the G376D variant had only a very minor effect (Fig. 5A and B). Importantly, this observation was not limited to overexpression in HEK293T cells: it was also confirmed in U2OS cell lines stably expressing doxycycline-inducible wild-type, G376V and G376D TDP-43 (Supplementary Fig. 5).



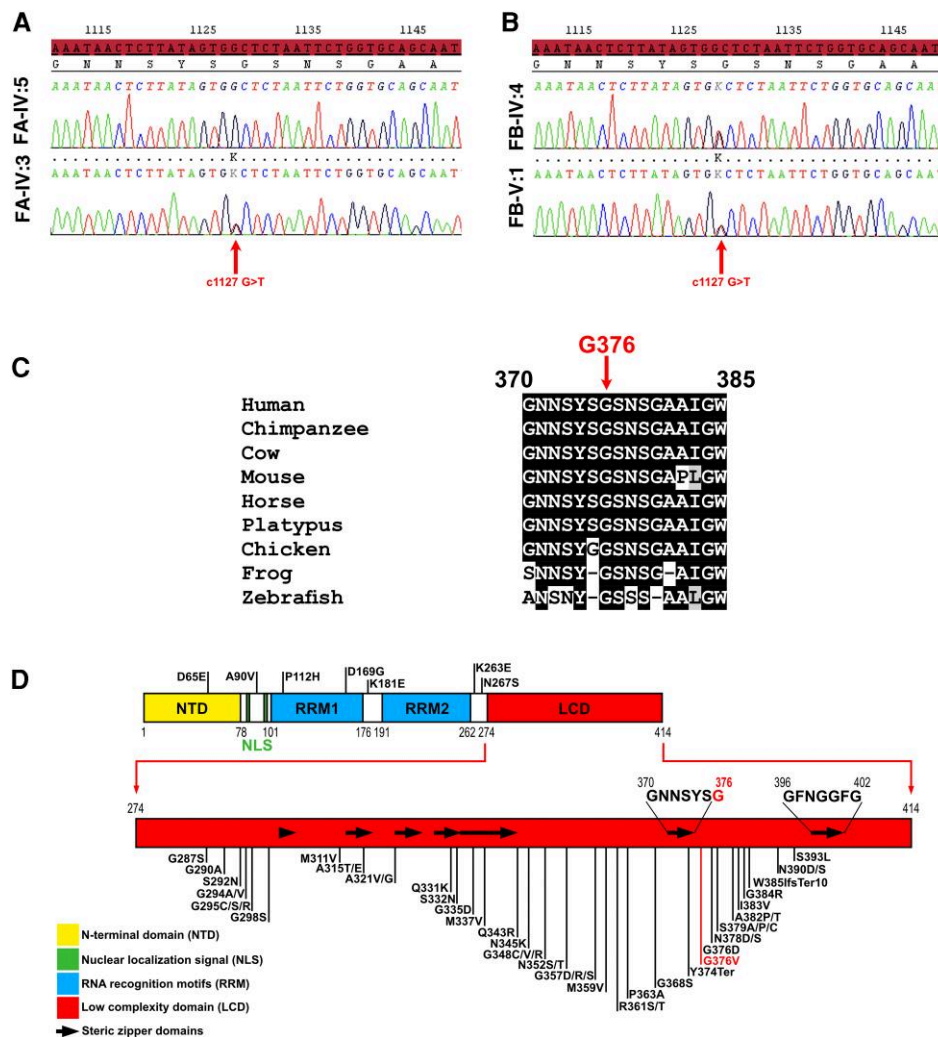


**Figure 3 Identification of the G376V-TDP-43 variant.** (A and B) Sanger sequencing chromatograms. (A) TARDBP sequence around codon 376 in non-affected Individual FA-IV:5 and affected Patient FA-IV:3 from Family A. (B) TARDBP sequence around codon 376 in affected Patients FB-IV:4 and FB-V:1 from Family B. Note the heterozygous c.1127G>T substitution in the sequences obtained from affected individuals (arrow) corresponding to the G376V substitution in the TDP-43 protein. (C) Alignments of partial sequence of TDP-43 from multiple species. The arrow indicates the glycine residue (G) at position 376. Human (*Homo sapiens*): Q13148, chimpanzee (*Pan troglodytes*): H2PY00, mouse (*Mus musculus*): Q921F2, cow (*Bos taurus*): G3MX91, horse (*Equus caballus*): F6WAU6, platypus (*Ornithorhynchus anatinus*): F7EDX1, chicken (*Gallus gallus*): Q5ZLN5, frog (*Xenopus laevis*): A0A8J0TE74 and zebrafish (*Danio rerio*): NP\_958884. (D) Schematic representation of the full-length TDP-43 protein (adapted from Guenther et al.<sup>49</sup>) and positions of disease-associated variants. The G376V variant is highlighted in red. The low complexity domain (LCD) has been expanded in the figure, displaying peptide sequences and the relative positions of steric zipper segments for which information on the structure was available (black arrows/arrowhead). NLS = nuclear localization sequence; NTD = N-terminal domain; RRM = RNA-recognition motif.

To further compare properties of G376V- and G376D-mutant TDP-43, we performed similar *in vitro* experiments, as described above using recombinant purified wild-type, G376V and G376D proteins (Supplementary Fig. 3A and B). Bright-field microscopy revealed that phase separation behaviour of G376D-TDP-43 was largely indistinguishable from the wild-type in terms of size and roundness of condensates (Fig. 5C and D), while G376V-TDP-43 again yielded smaller and more irregularly, amorously shaped condensates. We also performed an *in vitro* aggregation experiment, in which fluorescently labelled TDP-43 is vigorously agitated in an aggregation-promoting buffer for 30 min, incubated for 2 or 4 h and then imaged by confocal microscopy.<sup>44</sup> In this assay, the G376V, but not the G376D mutant, showed more abundant and larger aggregates at earlier timepoint (2 h), suggesting that the kinetics of TDP-43 aggregation is accelerated by the G376V mutation (Fig. 5E and F).

In another series of experiments, we compared effects of G376V to further ALS-related missense variants. After sarkosyl treatment, variants tended to accumulate in the sarkosyl-insoluble fraction, but not to the extent seen for G376V (Supplementary Fig. 6). The only exception was the variant M337V, which had a more prominent effect (Supplementary Fig. 6A and B). Finally, we conducted fluorescence confocal imaging of HEK293T cells expressing GFP-tagged TDP-43 species. In the presence of sorbitol, an osmotic stressor that directs TDP-43 to stress granules,<sup>50,51</sup> the number of cytoplasmic TDP-43 condensates was substantially increased in cells expressing G376V-TDP-43 compared to cells transfected with GFP-tagged wild-type TDP-43. ALS-related variants G294A, G298S and Q331K also increased formation of cytoplasmic condensates; however, the effect was less prominent compared to G376V (Supplementary Fig. 6C–E). Western blotting revealed similar protein levels of overexpressed TDP-43 species (Supplementary Fig.

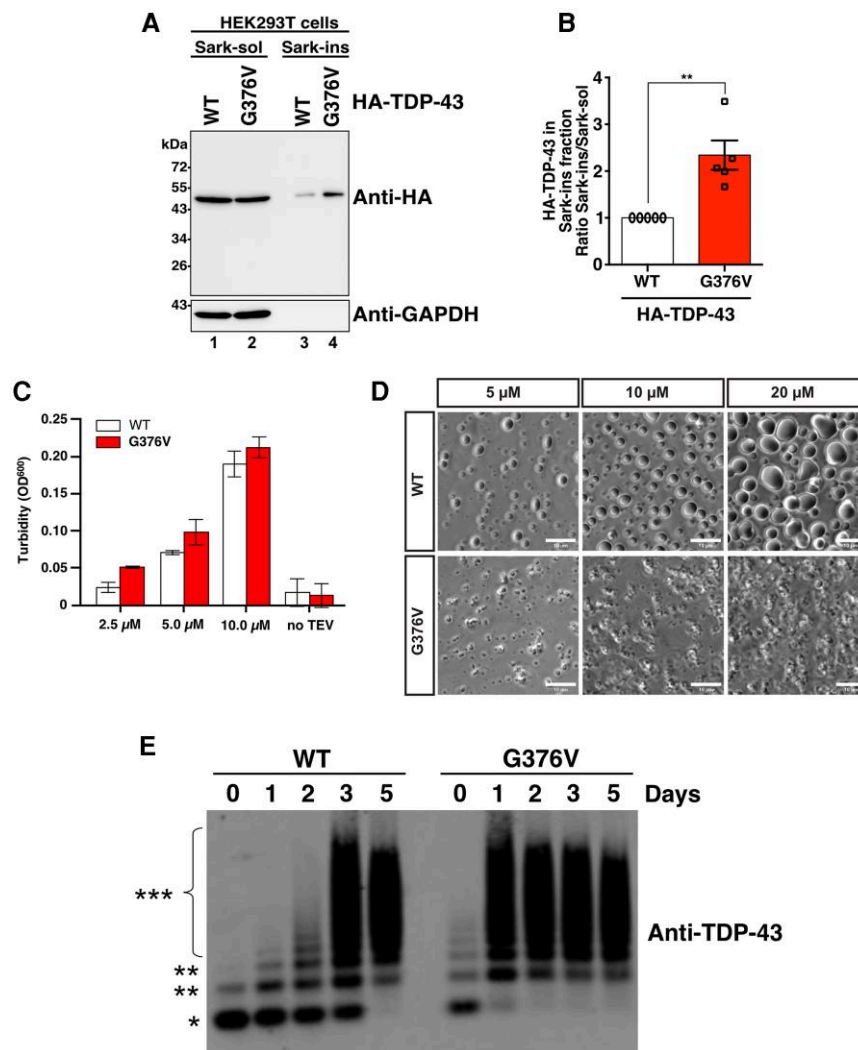


**Figure 4** Impact of the G376V variant on TDP-43 aggregation. (A) Immunoblotting of sarkosyl-soluble (Sark-sol) and sarkosyl-insoluble pellet (Sark-ins) fractions. Proteins were isolated from HEK293T cells expressing HA-tagged wild-type TDP-43 or the G376V variant. Anti-HA and anti-GAPDH antibodies were used for the detection of TDP-43-HA fusion proteins and the detection of GAPDH (loading control), respectively. (B) Ratios of wild-type and G376V variant HA-TDP-43 in the Sark-ins fraction to the Sark-sol fraction. The graphs represent mean  $\pm$  standard error of the mean (SEM) of  $n = 5$  experiments. All values were normalized to the mean of wild-type HA-TDP-43. Statistical significance was determined using an unpaired two-tailed Mann-Whitney test.  $**P = 0.0079$ . (C) Turbidity measurement (OD<sub>600</sub>) of wild-type (WT) and G376V-TDP-43 proteins (at 2.5, 5 or 10  $\mu\text{M}$ ) in solution. Wild-type and G376V-TDP-43-TEV-MBP-His<sub>6</sub> were purified from *Escherichia coli*. To trigger phase separation, the MBP-His<sub>6</sub> tag was removed by Tobacco Etch Virus (TEV) protease digestion. In the 'No TEV' control, the MBP-tag is retained, preventing TDP-43 phase separation. The graphs represent mean and  $\pm$  SEM of  $n = 3$  independent experiments. (D) Morphology of wild-type and G376V-TDP-43 condensates. Phase separation of recombinant TDP-43 proteins was induced and formation of condensates was analysed by phase contrast microscopy. Substitution of the glycine residue at position 376 by valine led to the formation of small amorphous condensates in a chain-like arrangement, while wild-type TDP-43 formed much larger, rounded, droplet-like condensates. Scale bars = 10  $\mu\text{m}$ . (E) Time course of the formation of high molecular weight TDP-43 species. Purified recombinant TDP-43-MBP-His<sub>6</sub> solutions were incubated for the indicated time periods (0 to 5 days), and formation of SDS-resistant high molecular weight TDP-43 species was visualized by semi-denaturing detergents agarose gel electrophoresis (SDD-AGE) and immunoblotting using an anti-TDP-43 antibody. \*Monomeric, \*\*oligomeric, \*\*\*polymeric forms of TDP-43.

6E), suggesting that the observed differences were not due to variable protein levels.

### G376V-TDP-43 forms more cytoplasmic condensates in sorbitol stressed patient-derived myoblasts and myotubes

We next investigated if aggregation of TDP-43 G376V was detectable in myoblasts and differentiated myotubes isolated from two patients carrying the G376V variant (Patients FA-IV:6 and FB-IV:4).

In the absence of the cellular stressor sorbitol, we failed to observe clear differences in the formation of cytoplasmic TDP-43 condensates between myoblasts from patients and control individuals (Controls CT1 and CT2) though there was a tendency for a higher rate of condensate formation in one patient (Patient FA-IV:6; [Supplementary Fig. 7A and B](#)). Similarly, no significant differences were observed in myotubes ([Supplementary Fig. 7C](#)). These results were largely consistent with prior research revealing the experimental challenges associated with visualizing TDP-43 condensates in cultured cells derived from affected patients.<sup>58</sup> As TDP-43

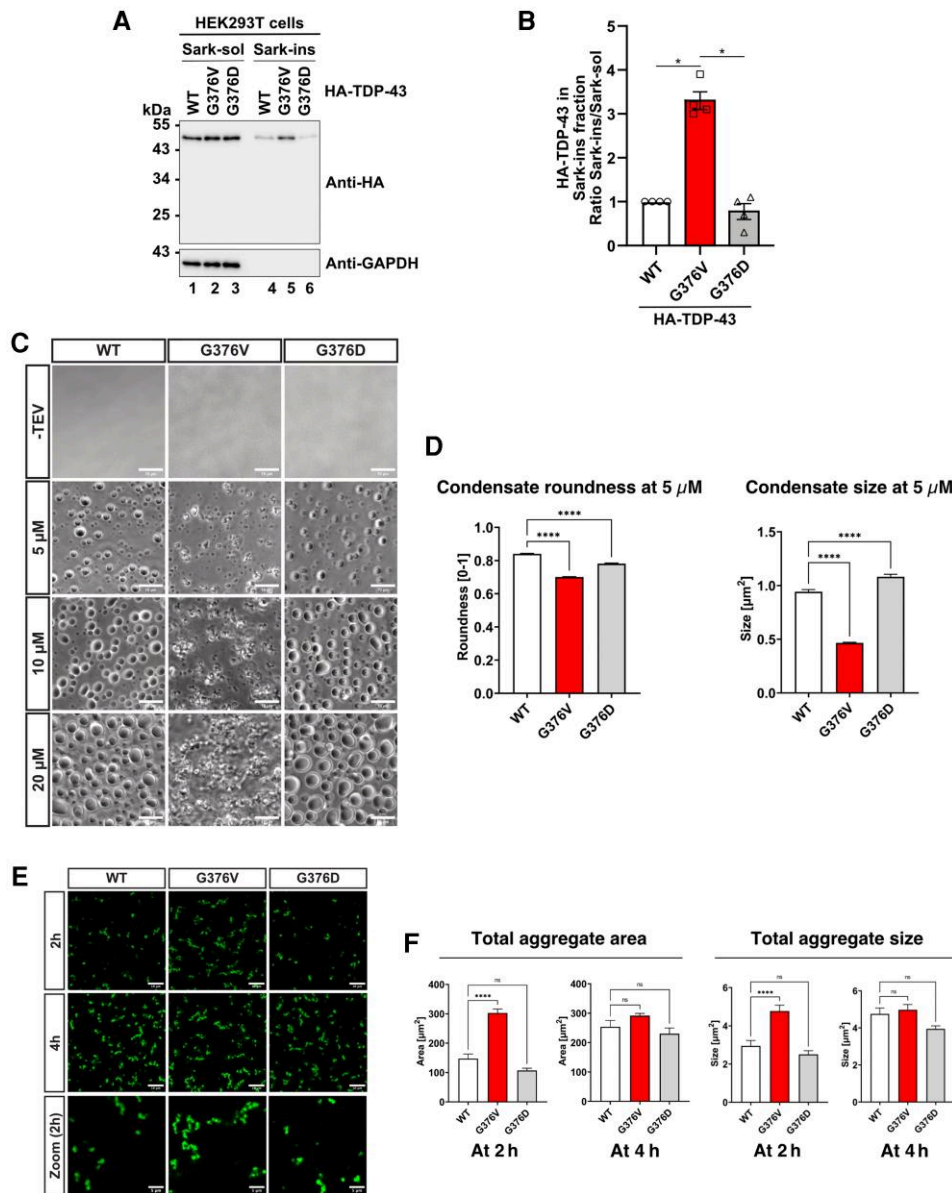


**Figure 5** Comparisons of aggregation and aggregation propensity of G376V and G376D-TDP-43. (A) Immunoblotting of sarkosyl-soluble (Sark-sol) and sarkosyl-insoluble (Sark-ins) fractions. Proteins were isolated from HEK293T cells expressing HA-tagged wild-type (WT) TDP-43 or the G376V or the G376D variants. Anti-HA and anti-GAPDH antibodies were used for the detection of TDP-43-HA fusion proteins and the detection of GAPDH (loading control), respectively. (B) Ratios of wild-type and G376V or G376D HA-TDP-43 in the Sark-ins fraction to the Sark-sol fraction. All values were normalized to the mean of wild-type HA-TDP-43. The graphs represent mean  $\pm$  standard error of the mean (SEM) of  $n = 4$  experiments. Significance was assessed using a Mann–Whitney test ( $*P < 0.05$ ). (C) Morphology of wild-type, G376V-TDP-43 and G376D-TDP43 condensates analysed by phase contrast microscopy. The G376V variant formed small, amorphous condensates while wild-type TDP-43 and G376D-TDP-43 formed large rounded, droplet-like condensates. Scale bars = 10  $\mu\text{m}$ . (D) Quantification of condensate roundness and size at 5  $\mu\text{M}$ . Bar graphs represent a minimum of two fields of view (FOV) ( $\sim 2000$  condensates each)  $\pm$  SEM. Statistical significance was determined using a one-way ANOVA with a multiple comparisons Dunnett's test to wild-type ( $****P < 0.0001$ ). (E) Confocal images of Alexa488-labelled TDP-43 aggregates formed in an *in vitro* aggregation assay [with Tobacco Etch Virus (TEV) protease cleavage of the indicated recombinant protein] at 2 and 4 h. Scale bars = 10  $\mu\text{m}$ . Zoom shows magnified view of aggregates at the 2 h time point. Scale bars = 5  $\mu\text{m}$ . (F) Quantification of the total aggregate area (in  $\mu\text{m}^2$ ) and total aggregate size (in  $\mu\text{m}^2$ ) shown in bar graphs as means of a minimum of nine FOV from three replicates per condition  $\pm$  SEM. Statistical significance was determined using a one-way ANOVA with a multiple comparisons Dunnett's test to wild-type ( $****P < 0.0001$ ).

condensate can be stimulated by using chemical stressors, such as proteasome inhibitors, sodium arsenite or sorbitol,<sup>23,58,62,63</sup> we treated myoblasts and myotubes with sorbitol to induce hyperosmotic stress. This experimental approach revealed an increase of TDP-43-positive cytoplasmic condensates in myoblasts and myotubes from both patients carrying the G376V variant but not in non-disease controls (Fig. 6A–C).

### Altered pre-mRNA splicing occurs in patient-derived G376V mutant muscle tissue

A major function of TDP-43 is to repress the inclusion of non-conserved cryptic exons during RNA splicing in order to maintain integrity of the open reading frame.<sup>64,65</sup> In pathological contexts, when TDP-43 is depleted from the nucleus or abnormally

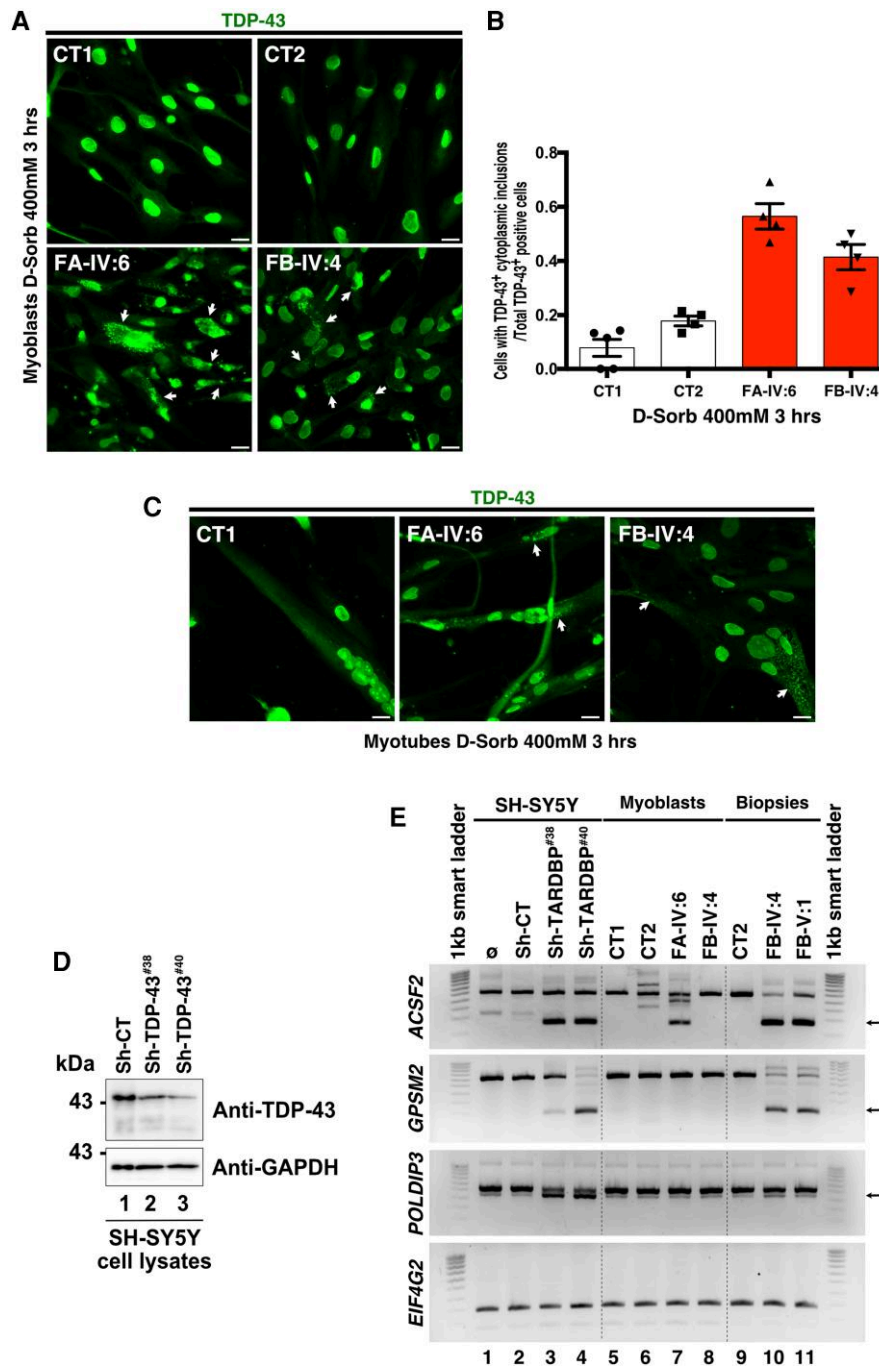


**Figure 6** TDP-43 condensates and irregular splicing in biomaterials of patients with the G376V-TDP-43 variant. (A) Condensate formation in myoblasts. Primary myoblasts isolated from non-disease control individuals (Controls CT1, CT2) or from patients with the G376V-TDP-43 variant (Patients FA-IV:6 and FB-IV:4) were cultured in the presence of sorbitol (400 mM) for 3 h and subsequently analysed by confocal immunofluorescence (IF) microscopy using an anti-TDP-43 antibody. White arrows indicate cytoplasmic TDP-43 inclusions. Scale bars = 20 μm. (B) The ratio of cells with cytoplasmic TDP-43 inclusions to all TDP-43 positive cells was determined in four randomly selected 20 × visual fields per condition and is given as mean ± SEM. (C) Aggregate formation in myotubes. Primary myoblasts from a non-disease control individual (Control CT1) or affected patients (Patients FA-IV:6 and FB-IV:4) were differentiated into myotubes, cultured in the presence of osmotic stress, as described above, and analysed by confocal IF microscopy using an anti-TDP-43 antibody. White arrows indicate cytoplasmic TDP-43 inclusions. Scale bars = 20 μm. (D) TDP-43 western blotting of SH-SY5Y neuroblastoma cells transduced with lentivectors expressing control small hairpin interference RNA (ShRNA CT) or ShRNAs directed against TARDBP (ShTARDBP#38 and #40). GAPDH was used as loading control. (E) Splicing of ACSF2, GPSM2 and POLDIP3-exon 3 but not EIF4G2 is altered in SH-SY5Y TDP-43 knock down cells and in muscle tissue of patients with the G376V TDP-43 variant. SH-SY5Y cells: Lane 1: non-transduced cells; Lane 2: Sh-CT cells; Lanes 3 and 4: two independent TARDBP ShRNAs (#38 and #40). Control and G376V patient myoblasts: Lanes 5 and 6: control myoblasts CT1 and CT2; Lanes 7 and 8: G376V myoblasts from Patients FA-IV:6 and FB-IV:4. Muscle biopsies: Lane 9: control muscle biopsy CT2; Lanes 10 and 11: muscle biopsies from Patients FB-IV:4 and FB-V:1. *Far left and right lanes*: 1 kb DNA ladder. Expected sizes of transcripts containing cryptic exons (arrows): ACSF2: 169 bp; GPSM2: 199 bp and POLDIP3: 392–400 bp.

accumulating in cytoplasmic or nuclear inclusions, its splicing repressor activity is compromised resulting in the incorporation of deleterious cryptic exons.<sup>66–71</sup> Recent studies revealed inclusion of cryptic exons in transcripts also from muscle cells and tissues when nuclear TDP-43 was depleted and shifted into cytoplasmic aggregates.<sup>72,73</sup> These results prompted us to perform RT-PCR experiments for three previously validated TDP-43 target genes, *ACSF2*, *GPSM2* and *POLDIP3*,<sup>72,73</sup> using mRNAs from control and G376V-TDP-43 mutant muscle biopsies (Control CT2 and Patients FB-IV:4 and FB-V:1). TDP-43 knockdown (KD) SH-SY5Y cells served as positive control (Fig. 6D). Similar splicing alterations of *ACSF2*, *GPSM2* and *POLDIP3* were observed in the SH-SY5Y TDP-43 KD cells and patient-derived muscle biopsies, while SH-SY5Y cells treated with non-targeting scramble shRNA and non-disease control muscle biopsies showed regular splicing patterns (Fig. 6E). No alteration of splicing was observed in the *EIF4G2* gene, which is known not to be a target gene for TDP-43. The analogous experiment in myoblasts yielded no abnormal splicing patterns in patient-derived myoblasts compared to non-disease controls, except for the *ACSF2* gene in one pathologic sample (Patient FA-IV:6; Fig. 6E). The negative results in myoblasts are in agreement with the virtual absence of cytoplasmic TDP-43 inclusions in unstressed patient-derived myoblasts.

## Discussion

In the present study, we identified a G376V-TDP-43 variant in patients with late-onset distal myopathy devoid of motor neuron disease. We also found that the G376V variant altered the behaviour of TDP-43: the mutant protein was more prone to aggregation, formed abnormal condensates *in vitro*, mislocalized to the cytoplasm in patient-derived muscle cells, and altered mRNA splicing in diseased muscle tissue.

The clinical presentation of patients with the G376V-TDP-43 variant was rather homogenous, with onset after 50 years of age, often asymmetric distribution, preferential involvement of the muscles in the anterior compartment of the forearm, and spreading to all four extremities within 5–10 years. During the course of the disease, most patients experienced involvement of bulbar and respiratory musculature. EMG, muscle MRI and muscle biopsy findings were consistent with a primary skeletal muscle disease. Conversely, we found no evidence of a devastating motor neuron disease, such as ALS. The disease had a chronic course, progressing slowly over several decades. Affected individuals usually maintained their ability to walk and did not require nutritional or ventilatory support during the day. Moreover, there were no indications of lower motor neuron involvement, such as fasciculations, abnormal EMG readings or neurogenic atrophy in biopsy samples. Likewise, there were no signs of upper motor neuron involvement, such as spasticity, exaggerated reflexes or abnormal plantar responses. Upon neurological examination, none of the patients displayed overt symptoms of dementia, and there were no self-reported cognitive issues or problems reported by relatives or partners.

Three patients had varying forms of heart disease. Given the absence of a consistent pattern of cardiac involvement and considering the patients' high risk for cardiovascular morbidity due to their age, we did not find a clear association between TDP-43-related myopathy and heart disease. However, one cannot fully rule out this possibility because a broad range of cardiac abnormalities can be linked with primary (hereditary) myopathies.<sup>74</sup>

The c.1127G>T (G376V) variant co-segregated with the disease phenotype in both families except for Individual FA-III:6, who carried the G376V variant but was reportedly unaffected at the age of 75. This observation was consistent with incomplete penetrance, which has been previously reported in TARDBP-related ALS.<sup>6</sup> The pathogenic relevance of the G376V variant was further underpinned by the fact that genes related to known causes of distal myopathies were largely excluded by exome sequencing and previous Sanger sequencing studies in both families, as well as genome-wide linkage analysis in Family A. Identification of a TARDBP variant related to a hereditary myopathy may also help resolving the long-debated question of whether TDP-43 positive inclusions observed in myofibres in various skeletal muscle disorders, such as myofibrillary or vacuolar myopathies,<sup>32,75</sup> represent a common end point of muscle cell degeneration or are at the crux of the disease mechanism. Our findings support the latter idea and imply that mutant TDP-43, in an unstable thermodynamic status, is not an innocent bystander and can directly cause skeletal muscle pathology. This interpretation is in agreement with observations in TDP-43-overexpressing transgenic mice, which displayed elevated CK levels and muscle histology with myopathic changes associated with TDP-43 aggregation.<sup>76</sup>

Like almost all ALS-linked TARDBP variants, the myopathy-associated G376V variant is localized in the PrLD/LCD domain.<sup>6</sup> Notably, a glycine to aspartic acid substitution affecting the same codon (G376D) has been previously reported in patients with rapidly progressive ALS.<sup>51–59</sup> The glycine residue at position 376 is highly conserved and glycine is the smallest and the most flexible amino acid. This feature could be essential for protein conformation and might be required for protein function and interactions. Substituting G376 with either valine (higher hydrophobicity) or aspartic-acid (negatively charged) may lead to the formation or destabilization of hydrogen or hydrophobic bonds, which may alter the steric environment or intra- and intermolecular interactions with surrounding amino acids or other TDP-43 molecules. This hypothesis is in agreement with recent structural data for the TDP-43 LCD, which implies that substitutions like G376D cause steric clashes within tightly packed segments of the protein.<sup>77</sup> Such changes are likely to disrupt the normal TDP-43 LCD structure, potentially resulting in abnormal formation of fibrillar structures, as previously depicted for different ALS-variants targeting the TDP-43 LCD domain.<sup>50</sup>

During the preparation of our manuscript, another study was published, reporting a single family with autosomal dominant myopathy caused by a TARDBP frameshift variant (W385IfsTer10), which was distinct from the missense variants typically found in individuals with TDP-43-related motor neuron disease.<sup>78</sup> This observation suggested that different types of mutations might determine whether myopathy or motor neuron disease manifests. However, our research demonstrated that a missense variant, similar to previously reported ALS-related variants, can also cause a myopathy. In line with computational predictions, the G376V variant exhibited an increased propensity for TDP-43 aggregation and led to the formation of more amorphous condensates through phase separation. Interestingly, the ALS-associated G376D variant, affecting the same G376 amino acid residue, displayed a behaviour that was very similar to the wild-type TDP-43, with lower aggregation tendencies and formation of very round, droplet-like condensates. It could be speculated that these observed differences might account for why G376V leads to myopathy, while G376D results in ALS. However, prior studies have indicated that several other ALS-associated TDP-43 variants behaved similarly to

G376V.<sup>6,11,13,14</sup> This suggests that there are diverse underlying pathomechanisms for TDP-43 mutations, potentially linked to clinical phenotypes, rather than a dichotomy of mechanisms resulting in either muscle or motor neuron disease. Actually, the causes behind the distinctive muscle-specific and brain-specific pathologies resulting from G376V and G376D variants may encompass factors that have not been extensively recognized before. One potential explanation could be that G376D acts as a phosphomimetic variant, whereas G376V does not.<sup>42,79</sup> Disease-linked TDP-43 phosphorylation has recently garnered considerable attention as a potent modifier of TDP-43 pathology, preventing TDP-43 condensation and aggregation in cell and *in vitro* models.<sup>44</sup>

Despite intense research over the past 15 years, our understanding of how pathological aggregation of TDP-43 is initiated remains incomplete. However, it seems reasonable to assume that the interplay of accumulating internal factors (e.g. genetic variants) and environmental stressors (e.g. infectious pathogens) could modulate the aggregation process of TDP-43 over time and therefore the nature of the pathology.<sup>6,80</sup> Similar to observations in cancers or viral diseases, the presence or absence of cellular factors with suppressive or enhancer properties may play a role in determining the effects of TDP-43 variants on the tissue specificity and the course of the disease.<sup>81</sup> Genome-wide association studies (GWAS) conducted in large ALS cohorts have unveiled numerous ALS-modifying genes that can modulate the progression of the disease.<sup>82</sup> Currently, it remains uncertain whether these genetic modifiers may also contribute to determination of the tissue-specificity of TARDBP variants, such as G376V.

Several recent studies reported that nuclear depletion and cytoplasmic aggregation of TDP-43 compromise splicing repressor activity of TDP-43. This has been shown to result in the emergence of abnormal splicing of TDP-43 target genes, promoting nonsense-mediated decay, loss of protein expression, or protein synthesis from illegitimate transcripts containing cryptic exons.<sup>66-71</sup> Indeed, we observed altered splicing patterns for ACSF2, GPSM2 and POLDIP3 genes in muscle biopsies from patients with the G376V variant. Interestingly, the previously reported myopathy-related TDP-43 variant<sup>78</sup> appears to alter splicing of mRNAs coding for muscle-specific structural and contraction-associated proteins. It seems reasonable to assume that such alterations may contribute to tissue tropism of TARDBP variants. Nevertheless, due to the multitude of cellular processes in which TDP-43 is involved, it remains speculative whether altered splicing is the core pathology or if another mechanism could be equally or even more pathogenetically relevant.

Taken together, our study demonstrates that TARDBP variants are not limited to rapidly progressive, fatal neurodegenerative disorders but can also lead to late-onset, chronic myopathies. Understanding the molecular and cellular mechanisms related to the pleiotropic effects of TARDBP variants could shed light on the underlying pathomechanisms and guide the identification of potential therapeutic targets in the future.

## Data availability

Raw data of gels and immunoblot presented in this study are available in the [Supplementary material](#) or from the corresponding authors upon reasonable request.

## Acknowledgements

We thank the families for their participation in this study. We are grateful to Dieter Edbauer, Bjarne Udd, Tanya Stojkovic, Martin

Moussy and Bettina Schmid for insightful discussions. We thank Nora Knabe for help with generating the TDP-43-MBP-His<sub>6</sub> G376D expression construct and purification of G376D mutant protein.

## Funding

The project was supported by the CNRS and the INSERM, the AFM Téléthon through the MyoNeurALP strategic grant (to L.S. and P.L.), the French National agency for research ANR project SpreadALS (to F.P. and P.L.), the Fondation pour la Recherche Médicale through an équipe FRM grant to L.S., the FILSLAN (to F.P. and P.L.), the Association pour la Recherche sur la SLA (ARSLA to P.L.), the German Federal Ministry of Education and Research (BMBF) through the German Network for Charcot-Marie-Tooth neuropathies (CMT-NET) (01GM1511B; to J.S.), and the Fritz-Thyssen-Stiftung (Az.10.15.1.021MN; to J.S.), the German Research Foundation (DFG) within the SPP2191 (project number 419139133; to D.D.), Heisenberg grant (project number 442698351, to D.D.) and the Munich Cluster of Systems Neurology (SyNergy, EXC2145, project number 390857198; to D.D. and .T.K.). Support by the IMB Microscopy Core Facility and use of a DFG-funded Confocal Laser Scanning Microscope (CLSM) with Fluorescence Lifetime Imaging Microscopy (FLIM) (project number 497669232, to Sandra Ritz/IMB) are gratefully acknowledged.

## Competing interests

The authors report no competing interests.

## Supplementary material

[Supplementary material](#) is available at *Brain* online.

## References

- Ling SC, Polymenidou M, Cleveland DW. Converging mechanisms in ALS and FTD: Disrupted RNA and protein homeostasis. *Neuron*. 2013;79:416-438.
- Versluys L, Ervilha Pereira P, Schuermans N, et al. Expanding the TDP-43 proteinopathy pathway from neurons to muscle: Physiological and pathophysiological functions. *Front Neurosci*. 2022;16:815765.
- Guo W, Chen Y, Zhou X, et al. An ALS-associated mutation affecting TDP-43 enhances protein aggregation, fibril formation and neurotoxicity. *Nat Struct Mol Biol*. 2011;18:822-830.
- Prasad A, Bharathi V, Sivalingam V, Girdhar A, Patel BK. Molecular mechanisms of TDP-43 misfolding and pathology in amyotrophic lateral sclerosis. *Front Mol Neurosci*. 2019;12:25.
- Zbinden A, Pérez-Berlangua M, De Rossi P, Polymenidou M. Phase separation and neurodegenerative diseases: A disturbance in the force. *Dev Cell*. 2020;55:45-68.
- Buratti E. Functional significance of TDP-43 mutations in disease. *Adv Genet*. 2015;91:25-53.
- Neumann M, Sampathu DM, Kwong LK, et al. Ubiquitinated TDP-43 in frontotemporal lobar degeneration and amyotrophic lateral sclerosis. *Science*. 2006;314:130-133.
- Nonaka T, Hasegawa M. TDP-43 Prions. *Cold Spring Harb Perspect Med*. 2018;8:a024463.
- Arai T, Hasegawa M, Akiyama H, et al. TDP-43 is a component of ubiquitin-positive tau-negative inclusions in frontotemporal lobar degeneration and amyotrophic lateral sclerosis. *Biochem Biophys Res Commun*. 2006;351:602-611.

10. Hasegawa M, Arai T, Nonaka T, et al. Phosphorylated TDP-43 in frontotemporal lobar degeneration and amyotrophic lateral sclerosis. *Ann Neurol*. 2008;64:60-70.
11. Conicella AE, Zerze GH, Mittal J, Fawzi NL. ALS mutations disrupt phase separation mediated by  $\alpha$ -helical structure in the TDP-43 low-complexity C-terminal domain. *Structure*. 2016;24:1537-1549.
12. Alberti S, Dormann D. Liquid-liquid phase separation in disease. *Annu Rev Genet*. 2019;53:171-194.
13. French RL, Grese ZR, Aligireddy H, et al. Detection of TAR DNA-binding protein 43 (TDP-43) oligomers as initial intermediate species during aggregate formation. *J Biol Chem*. 2019;294:6696-6709.
14. Johnson BS, Snead D, Lee JJ, McCaffery JM, Shorter J, Gitler AD. TDP-43 is intrinsically aggregation-prone, and amyotrophic lateral sclerosis-linked mutations accelerate aggregation and increase toxicity. *J Biol Chem*. 2009;284:20329-20339.
15. Sreedharan J, Blair IP, Tripathi VB, et al. TDP-43 mutations in familial and sporadic amyotrophic lateral sclerosis. *Science*. 2008;319:1668-1672.
16. Gitcho MA, Baloh RH, Chakraverty S, et al. TDP-43 A315T mutation in familial motor neuron disease. *Ann Neurol*. 2008;63:535-538.
17. Kabashi E, Valdmanis PN, Dion P, et al. TARDBP mutations in individuals with sporadic and familial amyotrophic lateral sclerosis. *Nat Genet*. 2008;40:572-574.
18. Posa D, Martínez-González L, Bartolomé F, et al. Recapitulation of pathological TDP-43 features in immortalized lymphocytes from sporadic ALS patients. *Mol Neurobiol*. 2019;56:2424-2432.
19. De Marco G, Lomartire A, Calvo A, et al. Monocytes of patients with amyotrophic lateral sclerosis linked to gene mutations display altered TDP-43 subcellular distribution. *Neuropathol Appl Neurobiol*. 2017;43:133-153.
20. Quek H, Cuní-López C, Stewart R, et al. ALS monocyte-derived microglia-like cells reveal cytoplasmic TDP-43 accumulation, DNA damage, and cell-specific impairment of phagocytosis associated with disease progression. *J Neuroinflammation*. 2022;19:58.
21. Romano N, Catalani A, Lattante S, et al. ALS skin fibroblasts reveal oxidative stress and ERK1/2-mediated cytoplasmic localization of TDP-43. *Cell Signal*. 2020;70:109591.
22. Riancho J, Castanedo-Vázquez D, Gil-Bea F, et al. ALS-derived fibroblasts exhibit reduced proliferation rate, cytoplasmic TDP-43 aggregation and a higher susceptibility to DNA damage. *J Neurol*. 2020;267:1291-1299.
23. Ratti A, Gumina V, Lenzi P, et al. Chronic stress induces formation of stress granules and pathological TDP-43 aggregates in human ALS fibroblasts and iPSC-motoneurons. *Neurobiol Dis*. 2020;145:105051.
24. Mori F, Tada M, Kon T, et al. Phosphorylated TDP-43 aggregates in skeletal and cardiac muscle are a marker of myogenic degeneration in amyotrophic lateral sclerosis and various conditions. *Acta Neuropathol Commun*. 2019;7:165.
25. Cykowski MD, Powell SZ, Appel JW, Arumanayagam AS, Rivera AL, Appel SH. Phosphorylated TDP-43 (pTDP-43) aggregates in the axial skeletal muscle of patients with sporadic and familial amyotrophic lateral sclerosis. *Acta Neuropathol Commun*. 2018;6:28.
26. Nelson PT, Lee EB, Cykowski MD, et al. LATE-NC staging in routine neuropathologic diagnosis: an update. *Acta Neuropathol*. 2023;145:159-173.
27. Josephs KA, Murray ME, Whitwell JL, et al. Staging TDP-43 pathology in Alzheimer's disease. *Acta Neuropathol*. 2014;127:441-450.
28. Rayaprolu S, Fujioka S, Traynor S, et al. TARDBP mutations in Parkinson's disease. *Parkinsonism Relat Disord*. 2013;19:312-315.
29. Weihl CC, Pestronk A, Kimonis VE. Valosin-containing protein disease: Inclusion body myopathy with Paget's disease of the bone and fronto-temporal dementia. *Neuromuscul Disord*. 2009;19:308-315.
30. Küsters B, van Hoeve BJA, Schelhaas HJ, Ter Laak H, van Engelen BGM, Lammens M. TDP-43 accumulation is common in myopathies with rimmed vacuoles. *Acta Neuropathol*. 2009;117:209-211.
31. Weihl CC, Temiz P, Miller SE, et al. TDP-43 accumulation in inclusion body myopathy muscle suggests a common pathogenic mechanism with frontotemporal dementia. *J Neurol Neurosurg Psychiatry*. 2008;79:1186-1189.
32. Olivé M, Janué A, Moreno D, Gámez J, Torrejón-Escribano B, Ferrer I. TAR DNA-Binding protein 43 accumulation in protein Aggregate myopathies. *J Neuropathol Exp Neurol*. 2009;68:262-273.
33. Salajegheh M, Pinkus JL, Taylor JP, et al. Sarcoplasmic redistribution of nuclear TDP-43 in inclusion body myositis. *Muscle Nerve*. 2009;40:19-31.
34. Nakamori M, Takahashi T, Nishikawa T, et al. Molecular markers for granulovacuolar degeneration are present in rimmed vacuoles. *PLoS One*. 2013;8:e80995.
35. Vogler TO, Wheeler JR, Nguyen ED, et al. TDP-43 and RNA form amyloid-like myo-granules in regenerating muscle. *Nature*. 2018;563:508-513.
36. Picchiarelli G, Dupuis L. Role of RNA binding proteins with prion-like domains in muscle and neuromuscular diseases. *CST*. 2020;4:76-91.
37. Svahn J, Coudert L, Streichenberger N, et al. Immune-Mediated rippling muscle disease associated with thymoma and anti-MURC/cavin-4 autoantibodies. *Neurol Neuroimmunol Neuroinflamm*. 2023;10:e200068.
38. Coudert L, Osseni A, Gangloff YG, Schaeffer L, Leblanc P. The ESCRT-0 subcomplex component Hrs/Hgs is a master regulator of myogenesis via modulation of signaling and degradation pathways. *BMC Biol*. 2021;19:153.
39. Nonaka T, Kametani F, Arai T, Akiyama H, Hasegawa M. Truncation and pathogenic mutations facilitate the formation of intracellular aggregates of TDP-43. *Hum Mol Genet*. 2009;18:3353-3364.
40. Nonaka T, Masuda-Suzukake M, Arai T, et al. Prion-like properties of pathological TDP-43 aggregates from diseased brains. *Cell Rep*. 2013;4:124-134.
41. Colombo M, Moita C, van Niel G, et al. Analysis of ESCRT functions in exosome biogenesis, composition and secretion highlights the heterogeneity of extracellular vesicles. *J Cell Sci*. 2013;126:5553-5565.
42. Wang A, Conicella AE, Schmidt HB, et al. A single N-terminal phosphomimic disrupts TDP-43 polymerization, phase separation, and RNA splicing. *EMBO J*. 2018;37:e97452.
43. Coudert L, Nonaka T, Bernard E, Hasegawa M, Schaeffer L, Leblanc P. Phosphorylated and aggregated TDP-43 with seeding properties are induced upon mutant Huntingtin (mHtt) polyglutamine expression in human cellular models. *Cell Mol Life Sci*. 2019;76:2615-2632.
44. Da Silva LA G, Simonetti F, Hutten S, et al. Disease-linked TDP-43 hyperphosphorylation suppresses TDP-43 condensation and aggregation. *EMBO J*. 2022;41:e108443.
45. Hutten S, Usluer S, Bourgeois B, et al. Nuclear import receptors directly bind to arginine-rich dipeptide repeat proteins and suppress their pathological interactions. *Cell Rep*. 2020;33:108538.
46. Karczewski KJ, Francioli LC, Tiao G, et al. The mutational constraint spectrum quantified from variation in 141,456 humans. *Nature*. 2020;581:434-443.
47. Fu W, O'Connor TD, Jun G, et al. Analysis of 6,515 exomes reveals the recent origin of most human protein-coding variants. *Nature*. 2013;493:216-220.

48. Sudmant PH, Rausch T, Gardner EJ, et al. An integrated map of structural variation in 2,504 human genomes. *Nature*. 2015; 526:75-81.
49. Guenther EL, Cao Q, Trinh H, et al. Atomic structures of TDP-43 LCD segments and insights into reversible or pathogenic aggregation. *Nat Struct Mol Biol*. 2018;25:463-471.
50. Zhou X, Sumrow L, Tashiro K, et al. Mutations linked to neurological disease enhance self-association of low-complexity protein sequences. *Science*. 2022;377:eabn5582.
51. Ruffo P, Catalano S, La Bella V, Conforti FL. Deregulation of plasma microRNA expression in a TARDBP-ALS family. *Biomolecules*. 2023;13:706.
52. D'Anzi A, Altieri F, Perciballi E, et al. Generation of an induced pluripotent stem cell line (CSS012-A (7672)) carrying the p.G376D heterozygous mutation in the TARDBP protein. *Stem Cell Res*. 2021;53:102356.
53. D'Anzi A, Perciballi E, Ruotolo G, et al. Production of CSSi013-A (9360) iPSC line from an asymptomatic subject carrying a heterozygous mutation in TDP-43 protein. *Stem Cell Res*. 2022;63: 102835.
54. Czell D, Andersen PM, Morita M, Neuwirth C, Perren F, Weber M. Phenotypes in Swiss patients with familial ALS carrying TARDBP mutations. *Neurodegener Dis*. 2013;12:150-155.
55. Lattante S, Sabatelli M, Bisogni G, et al. Evaluating the contribution of the gene TARDBP in Italian patients with amyotrophic lateral sclerosis. *Euro J Neurol*. 2023;30:1246-1255.
56. Mitsuzawa S, Akiyama T, Nishiyama A, et al. TARDBP p.G376D mutation, found in rapid progressive familial ALS, induces mislocalization of TDP-43. *eNeurologicalSci*. 2018;11:20-22.
57. Romano R, De Luca M, Del Fiore VS, et al. Allele-specific silencing as therapy for familial amyotrophic lateral sclerosis caused by the p.G376D TARDBP mutation. *Brain Commun*. 2022;4:fcac315.
58. Solski JA, Yang S, Nicholson GA, et al. A novel TARDBP insertion/deletion mutation in the flail arm variant of amyotrophic lateral sclerosis. *Amyotroph Lateral Scler*. 2012;13:465-470.
59. Conforti FL, Sproviero W, Simone IL, et al. TARDBP gene mutations in south Italian patients with amyotrophic lateral sclerosis. *J Neurol Neurosurg Psychiatry*. 2011;82:587-588.
60. Lancaster AK, Nutter-Upham A, Lindquist S, King OD. PLAAC: A web and command-line application to identify proteins with prion-like amino acid composition. *Bioinformatics*. 2014;30: 2501-2502.
61. Goldschmidt L, Teng PK, Riek R, Eisenberg D. Identifying the amyloids, proteins capable of forming amyloid-like fibrils. *Proc Natl Acad Sci U S A*. 2010;107:3487-3492.
62. Dewey CM, Cenik B, Sephton CF, Johnson BA, Herz J, Yu G. TDP-43 aggregation in neurodegeneration: are stress granules the key? *Brain Res*. 2012;1462:16-25.
63. Dewey CM, Cenik B, Sephton CF, et al. TDP-43 is directed to stress granules by sorbitol, a novel physiological osmotic and oxidative stressor. *Mol Cell Biol*. 2011;31:1098-1108.
64. Mehta PR, Brown AL, Ward ME, Fratta P. The era of cryptic exons: Implications for ALS-FTD. *Mol Neurodegener*. 2023;18:16.
65. Akiyama T, Koike Y, Petrucelli L, Gitler AD. Cracking the cryptic code in amyotrophic lateral sclerosis and frontotemporal dementia: Towards therapeutic targets and biomarkers. *Clin Transl Med*. 2022;12:e818.
66. Ling JP, Pletnikova O, Troncoso JC, Wong PC. TDP-43 repression of nonconserved cryptic exons is compromised in ALS-FTD. *Science*. 2015;349:650-655.
67. Brown AL, Wilkins OG, Keuss MJ, et al. TDP-43 loss and ALS-risk SNPs drive mis-splicing and depletion of UNC13A. *Nature*. 2022; 603:131-137.
68. Ma XR, Prudencio M, Koike Y, et al. TDP-43 represses cryptic exon inclusion in the FTD-ALS gene UNC13A. *Nature*. 2022; 603:124-130.
69. Donde A, Sun M, Ling JP, et al. Splicing repression is a major function of TDP-43 in motor neurons. *Acta Neuropathol*. 2019; 138:813-826.
70. Seddighi S, Qi YA, Brown AL, et al. Mis-spliced transcripts generate de novo proteins in TDP-43-related ALS/FTD. *Sci Transl Med*. 2024;16:eadg7162.
71. Torres P, Ramírez-Núñez O, Romero-Guevara R, et al. Cryptic exon splicing function of TARDBP interacts with autophagy in nervous tissue. *Autophagy*. 2018;14:1398-1403.
72. Britson KA, Ling JP, Braunstein KE, et al. Loss of TDP-43 function and rimmed vacuoles persist after T cell depletion in a xenograft model of sporadic inclusion body myositis. *Sci Transl Med*. 2022;14:eabi9196.
73. Šušnjar U, Škrabar N, Brown AL, et al. Cell environment shapes TDP-43 function with implications in neuronal and muscle disease. *Commun Biol*. 2022;5:314.
74. Finsterer J, Stöllberger C. Cardiac involvement in primary myopathies. *Cardiology*. 2000;94:1-11.
75. Goebel HH. Protein aggregate myopathies. Introduction. *Brain Pathol*. 2009;19:480-482.
76. Tawara N, Yamashita S, Kawakami K, et al. Muscle-dominant wild-type TDP-43 expression induces myopathological changes featuring tubular aggregates and TDP-43-positive inclusions. *Exp Neurol*. 2018;309:169-180.
77. Li Q, Babinchak WM, Surewicz WK. Cryo-EM structure of amyloid fibrils formed by the entire low complexity domain of TDP-43. *Nat Commun*. 2021;12:1620.
78. Ervilha Pereira P, Schuermans N, Meylemans A, et al. C-terminal frameshift variant of TDP-43 with pronounced aggregation-propensity causes rimmed vacuole myopathy but not ALS/FTD. *Acta Neuropathol*. 2023;145:793-814.
79. Paron F, Barattucci S, Cappelli S, et al. Unraveling the toxic effects mediated by the neurodegenerative disease-associated S375G mutation of TDP-43 and its S375E phosphomimetic variant. *J Biol Chem*. 2022;298:102252.
80. Leblanc P, Vorberg IM. Viruses in neurodegenerative diseases: more than just suspects in crimes. Haigh CL, ed. *PLoS Pathog*. 2022;18:e1010670.
81. Willemse SW, Van Es MA. Susceptibility and disease modifier genes in amyotrophic lateral sclerosis: from genetic associations to therapeutic implications. *Curr Opin Neurol*. 2023;36:365-370.
82. Suzuki N, Nishiyama A, Warita H, Aoki M. Genetics of amyotrophic lateral sclerosis: seeking therapeutic targets in the era of gene therapy. *J Hum Genet*. 2023;68:131-152.